

# Optimal error estimate of an isoparametric upwind discontinuous Galerkin method for radiation transport equation on curved domains

Changhui Yao <sup>\*</sup>      Yunpan Ma <sup>†</sup>      Lingxiao Li <sup>‡</sup>

2026-02-20

## Abstract

This work investigates the isoparametric upwind discontinuous Galerkin method for solving the radiation transport equation defined on a bounded domain  $D$  with a piecewise  $C^{k+1}$  smooth curved boundary. An auxiliary mapping is constructed to approximate the original curved domain. The analysis delineates a high-order optimal convergence rate under the DG norm, which comprehensively balances the errors stemming from the numerical discretization and the geometric approximation. Two- and three-dimensional numerical experiments validate the theoretical results.

**Key words.** Radiation transport equation; Upwind discontinuous Galerkin method; Auxiliary mapping; Isoparametric auxiliary operator; Optimal convergence rate

## 1 Introduction

The radiation transport equation (RTE) describes the propagation of photons in scattering media and their interactions with matter, with significant applications in fields such as astrophysics, atmospheric science, and high energy density physics [22, 33, 35]. A simplified form of the stationary RTE can be derived for angular discretization by employing the discrete ordinates (SN) method [20]. In this paper, we consider the governing equation

$$\Omega \cdot \nabla I + \sigma I = f \text{ in } D, \quad I = g \text{ on } \Gamma^-, \quad (1.1)$$

where  $I$  is the radiation intensity,  $\sigma$  is a bounded absorption coefficient,  $\Omega$  is a constant unit discrete direction.  $D$  is a bounded curved domain with boundary  $\Gamma = \partial D$ ,  $\Gamma^- = \{x \in \Gamma : \Omega \cdot \mathbf{n}(x) < 0\}$  is the inflow part of the boundary  $\Gamma$ , and  $\mathbf{n}(x)$  is the unit outward normal vector to  $\Gamma$  at  $x \in \Gamma$ .

The discontinuous Galerkin (DG) method is widely recognized as a primary and highly efficient numerical methodology for discretizing the radiation transfer equation [14], owing to its inherent capability of handling solution discontinuities and complex geometries [32]. Its application to neutron transport problems was first established in the foundational 1974 paper by Reed and Hill [24]. Theoretically, the DG method has been shown to achieve a suboptimal  $L^2$  norm convergence rate of order  $\mathcal{O}(h^{k+\frac{1}{2}})$  on quasi-uniform straight meshes [9, 18, 30]. In particular, an improved rate of  $\mathcal{O}(h^{k+1})$  can be realized on certain structured mesh families [12, 31]. Therefore, under the assumption of a quasi-uniform meshes, the method exhibits an optimal  $\mathcal{O}(h^{k+\frac{1}{2}})$  order error convergence rate analogous to the discrete norm in [18, 29].

In contrast to the optimal convergence rate  $\mathcal{O}(h^{k+\frac{1}{2}})$  achievable by the discrete norm on quasi-uniform straight meshes, the presence of curved boundaries can compromise this order due to geometric error [11, 26]. This error arises from the mismatch between the straight computational mesh and the actual curved domain, analogous to the error incurred when linearly

<sup>\*</sup>C. Yao. School of Mathematics and Statistics, Zhengzhou University, 450001, Zhengzhou, China. (chyao@lsec.cc.ac.cn)

<sup>†</sup>Y. Ma. School of Mathematics and Statistics, Zhengzhou University, 450001, Zhengzhou, China. (yunpanma@gs.zzu.edu.cn)

<sup>‡</sup>L. Li (**Corresponding Author**). School of Mathematics and Statistics, Henan University, 475004, Kaifeng, China. (lilingxiao@lsec.cc.ac.cn)

interpolating a nonlinear function. To recover the same optimal convergence rate as polygonal domain case, higher-order geometric approximations are essential. Established techniques for this purpose include the isoparametric finite element method [7], isogeometric analysis [17], and nonuniform rational B-spline (NURBS) enhanced finite element method [34]. The integration of isoparametric finite elements for geometric representation [19] with DG finite elements for function discretization [3, 5] provides a powerful approach, which effectively balances geometric accuracy and numerical performance.

The isoparametric finite element method has been extensively studied for problems on curved domains. Its development spans from the foundational analysis of the Poisson equation [10] to applications in parabolic [28] and eigenvalue problems [21]. More recently, it has been successfully applied to the Maxwell equations [3] and parametric divergence-free FEM for 3D Stokes equations [26] on curved domains. Furthermore, an optimal-order error estimate is presented for the arbitrary-Lagrangian-Eulerian (ALE) finite element method for a parabolic equation in an evolving domain, using high-order isoparametric finite elements with flat simplices in the interior of the domain [25]. Despite its extensive history, the theoretical framework for symmetric elliptic systems [1, 3, 10, 21, 25] remains inadequate for RTE, a problem marked by its non-symmetric, first-order hyperbolic character. Consequently, the treatment of its critical inflow boundary conditions remains largely unexplored.

In this work, we develop a numerical method aimed at recovering and preserving the optimal convergence order for the RTE discretized on curved domains, utilizing the isoparametric mapping approach. This method is based on the construction of a isoparametric mapping  $F_h$  [23] from a straight reference domain to an computational domain, which conforms to the original domain closely. A crucial aspect of this approach is the control of the geometric approximation error to prevent it from dominating the total discretization error. To facilitate the error analysis, an auxiliary mapping from the original domain to the computational domain is introduced in [2, 23]. The error analysis centers on the deviation, measured in DG norm [29], of the numerical solution on computational domain from a suitably extended weak solution of the original problem [6, 10]. The theoretical framework is rigorously established by decomposing the total error into two parts. The first part is the approximation error of isoparametric finite element space, where we defined an isoparametric auxiliary operator based on the local projection operator of the finite element space. The second part is the consistency error of the upwind DG method for RTE on curved domain, which requires analysing the difference between the auxiliary mapping image of inflow boundary of the original domain and the inflow part of the computational domain.

The error estimation addresses two essential challenges which originate from the curved domain geometry and the hyperbolic nature of the RTE, respectively.

- Geometric inconsistency at the inflow boundary: The inflow boundary of the computational domain does not precisely coincide with the mapped inflow boundary of the original domain. The crucial step is to analyze the geometric approximation error which could reduce its effect on the overall discretization error.
- Constraints of the isoparametric finite element space: The existing convergence analysis for the RTE on straight meshes relies critically on two aspects, the closure property of the differential operator on polynomial spaces and the well-established theory for finite element approximation operators. Unfortunately, these foundational tools are no longer directly applicable under the isoparametric finite element space.

To overcome the difficulties, we sufficiently combine the classical geometric measure theory, the property of the auxiliary mapping, with the finite element method error analysis framework. Our work is devoted to resolving the geometric and analytical challenges highlighted above and providing optimal error estimate.

The remainder of the manuscript is structured as follows. Section 2 introduces the three key domains: the reference, approximate, and original domains, along with the auxiliary mapping and the isoparametric finite element space. The standard upwind flux discontinuous Galerkin discretization is then formulated to solve the stationary RTE on the computational domain. In Section 3, we present a theoretical analysis demonstrating that the proposed isoparametric DG method with upwind flux achieves the optimal convergence rate in the DG norm. Section 4 provides numerical experiments that confirm the theoretical results and illustrate the effectiveness of the approach. Concluding remarks are given in Section 5.

## 2 Isoparametric finite element method on curved mesh

Throughout this work, we use the classical Sobolev spaces. For a domain  $D$ , an integer  $m \geq 0$ , and  $1 \leq p \leq \infty$ ,  $W^{m,p}(D)$  denotes the space of functions in  $L^p(D)$  whose weak partial derivatives of order up to  $m$  also lie in  $L^p(D)$ . The standard norm and semi-norm on this space are denoted by  $\|\cdot\|_{W^{m,p}(D)}$  and  $|\cdot|_{W^{m,p}(D)}$ , respectively. The Hilbert space is denoted by  $H^m(D) = W^{m,2}(D)$  with norm  $\|\cdot\|_{H^m(D)}$  and semi-norm  $|\cdot|_{H^m(D)}$ , respectively. The notation  $a \lesssim b$  means that  $a \leq Cb$  holds for a constant  $C > 0$  which is independent of the mesh size  $h$ . Moreover, Euclidian norm of a vector  $\Omega \in \mathbb{R}^3$  will be denoted by  $\|\Omega\|$ .

### 2.1 Computational domain and auxiliary mapping

We consider a bounded curved domain  $D \subset \mathbb{R}^d (d = 2, 3)$  with a Lipschitz continuous and piecewise  $C^{k+1}$  smooth boundary  $\Gamma$ . To this end, we approximate  $D$  by a polyhedral domain  $\widehat{D}_h$ , which is equipped with a quasi-uniform and shape-regular tetrahedral subdivision  $\widehat{\mathcal{T}}_h$  of size at most  $h$  and is constructed via a piecewise linear interpolation of  $\partial D$  (Sec 4.7 in [7]). Moreover, we denote the boundary of  $\widehat{D}_h = \partial \widehat{D}_h$ . The mapping from this polyhedral domain to the original domain is denoted by  $F : \widehat{D}_h \rightarrow D$ .

To analysis the extent of approximation between  $D$  and  $\widehat{D}_h$ , we may make some reasonable assumptions [4, 5, 26]:

(H<sub>1</sub>) The mapping  $F : \widehat{D}_h \rightarrow D$  is piecewise  $C^{k+1}$  continuous:  $F|_{\widehat{K}} \in C^{k+1}(\widehat{K})$ ,  $\forall \widehat{K} \in \widehat{\mathcal{T}}_h$ , which satisfies  $F(\widehat{K}) = \widehat{K}$  if all vertices of  $\widehat{K}$  are located within the domain  $\widehat{D}_h$ .

(H<sub>2</sub>) Let  $\mathbb{J}_F$  denote the Jacobian matrix of  $F$ . Then there holds

$$\|\mathbb{I} - \mathbb{J}_F\|_{L^\infty(\widehat{D}_h)} \lesssim h.$$

(H<sub>3</sub>) The mapping  $F : \widehat{D}_h \rightarrow D$  is invertible, and let  $F^{-1}$  denote the inverse of  $F$ . Then there holds

$$\max_{\widehat{K} \in \widehat{\mathcal{T}}_h} (\|F\|_{W^{k+1,\infty}(\widehat{K})} + \|F^{-1}\|_{W^{k+1,\infty}(\widehat{K})}) \lesssim 1.$$

The stated assumptions are mild and are readily satisfied on condition that the mesh  $\widehat{\mathcal{T}}_h$  is sufficiently refined (see, e.g., [5]). Since  $\Gamma$  is piecewise  $C^{k+1}$  smooth, assumption (H<sub>1</sub>) inherently reflects the smoothness properties of the original boundary  $\Gamma$ . Assumption (H<sub>2</sub>) holds when the approximate boundary  $\widehat{\Gamma}_h$  adequately resolves the geometry of the curved boundary  $\Gamma$ . Indeed, for a sufficiently fine mesh  $\mathcal{T}_h$ , the Hausdorff distance between  $\Gamma$  and  $\widehat{\Gamma}_h$  is of order  $\mathcal{O}(h^2)$ . We also refer to the remarks following Eq.(5.11) in [4] for further elaboration. Furthermore, assumption (H<sub>3</sub>) requires that the operator  $F$  and its inverse  $F^{-1}$  remain uniformly bounded with respect to the mesh size  $h$ . This condition is reasonable in view of the geometric and functional consistency ensured by Assumptions (H<sub>1</sub>) and (H<sub>2</sub>).

For any  $\widehat{K} \in \widehat{\mathcal{T}}_h$ , let  $F_{\widehat{K}} \in \mathbb{P}_k(\widehat{K})$  be the  $k^{\text{th}}$  order lagrange interpolation of  $F|_{\widehat{K}}$ , where  $\mathbb{P}_k$  is the space of vector polynomials with degrees no more than  $k$ . The global interpolation  $F_h \in \mathbb{C}(\widehat{D}_h)$  is defined by

$$F_h = F_{\widehat{K}}, \quad \forall \widehat{K} \in \widehat{\mathcal{T}}_h.$$

It defines the computational domain  $D_h$  and a subdivision of it

$$\mathcal{T}_h = \{K = F_h(\widehat{K}) : \widehat{K} \in \widehat{\mathcal{T}}_h\}, \quad D_h = \text{interior} \left( \bigcup_{K \in \mathcal{T}_h} \overline{K} \right).$$

Moreover, we denote the boundary and inflow boundary of  $D_h$  as  $\Gamma, \Gamma_h^-$ , respectively, where

$$\Gamma_h = \partial D_h, \quad \Gamma_h^- = \{y \in \Gamma_h : \Omega \cdot \mathbf{n}_h(y) < 0\}.$$

Here  $\mathbf{n}_h(y)$  is the outer normal vector of  $\Gamma_h$  at point  $y$ . Corresponding, we define the inflow(outer) boundary for each element  $K \in \mathcal{T}_h : \partial_{-(+)}K = \{x \in \partial K : \Omega \cdot \mathbf{n}_h(x) < (>)0\}$ .

Combining the assumptions ( $H_1 \sim H_3$ ) with the standard error estimate of lagrange interpolation [7], we have

$$\|F_h - F\|_{W^{m,\infty}(\widehat{D})} \lesssim h^{k+1-m}, \quad m = 0, 1. \quad (2.1)$$

Denote the identity mapping as  $id$  and the auxiliary mapping  $\Phi_h = F_h \circ F^{-1} : D \rightarrow D_h$ , respectively, there holds

$$\begin{aligned} \|id - \Phi_h\|_{W^{m,\infty}(D)} &= \|(F - F_h) \circ F^{-1}\|_{W^{m,\infty}(D)} \\ &\leq \|F_h - F\|_{W^{m,\infty}(\widehat{D})} \|\mathbb{J}_F^{-1}\|^m \\ &\lesssim h^{k+1-m}, \quad m = 0, 1, \end{aligned} \quad (2.2)$$

which implies the boundedness of the jacobian matrix and its determinant estimates

$$\|\mathbb{J}_{\Phi_h(x)}\|_{W^{1,\infty}(D)} \lesssim 1, \quad \|\mathcal{J}_{\Phi_h(x)}\|_{W^{1,\infty}(D)} \lesssim 1. \quad (2.3)$$

## 2.2 Isoparametric finite element spaces of RTE

The finite element space on the reference mesh  $\widehat{\mathcal{T}}_h$  is defined as

$$\widehat{V}_{h,k} = \{\widehat{v}_h \in L^2(\widehat{D}_h) : \widehat{v}_h|_{\widehat{K}} \in P_k(\widehat{K}), \forall \widehat{K} \in \widehat{\mathcal{T}}_h\}.$$

Then, the corresponding isoparametric finite element space on  $\mathcal{T}_h$  is defined as [7]

$$V_{h,k} = \{\widehat{v}_h \circ F_h^{-1} : \widehat{v}_h \in \widehat{V}_{h,k}\}.$$

Remarkably, the space  $V_{h,k}$  does not have to be a space of polynomials, yet it remains finite-dimensional.

For  $m \geq 0$ , we introduce the broken Sobolev space equipped with the corresponding broken norms [14]

$$H^m(\mathcal{T}_h) = \{v \in L^2(D_h) : v|_K \in H^m(K), \forall K \in \mathcal{T}_h\},$$

with the associated broken  $H^m$  norm and the broken  $L^\infty$  norm defined respectively as

$$\|v\|_{H^m(\mathcal{T}_h)} = \left( \sum_{K \in \mathcal{T}_h} \|v\|_{H^m(K)}^2 \right)^{\frac{1}{2}}, \quad \|v\|_{L^\infty(\mathcal{T}_h)} = \max_{K \in \mathcal{T}_h} \|v\|_{L^\infty(K)}.$$

More generally, for any  $p \in [1, \infty]$ , the broken  $W^{m,p}(\mathcal{T}_h)$  space and its norms can be defined analogously.

To characterize the discontinuous nature of the solution across elements, we distinguish between the interior and exterior traces at element boundaries. For each element  $K \in \mathcal{T}_h$ , a face  $F \subset \partial K$ , and a function  $v \in H^1(\mathcal{T}_h)$ , the interior and exterior traces on  $F$  are denoted by  $v^+$  and  $v^-$ , respectively. Furthermore, the jump of  $v$  across  $F$  is defined as  $\llbracket v \rrbracket := v^+ - v^-$  if  $F$  is an inner face.

The standard upwind DG formulation of isoparametric finite element method for (1.1) is defined as follows: Find  $I_h \in V_{h,k}$  such that

$$\mathcal{B}(I_h, v_h) = l(v_h), \quad \forall v_h \in V_{h,k}, \quad (2.4)$$

where the bilinear form  $\mathcal{B}(\cdot, \cdot)$  with upwind flux and the linear functional  $l(\cdot)$  are defined respectively as

$$\begin{aligned} \mathcal{B}(I_h, v_h) &= \sum_{K \in \mathcal{T}_h} \left( \int_K (\Omega \cdot \nabla I_h + \sigma I_h) v_h dx \right) - \sum_{K \in \mathcal{T}_h} \left( \int_{\partial_- K \cap \Gamma_h^-} (\Omega \cdot \mathbf{n}_h) I_h^+ v_h^+ ds \right) \\ &\quad - \sum_{K \in \mathcal{T}_h} \left( \int_{\partial_- K / \Gamma_h} (\Omega \cdot \mathbf{n}_h) \llbracket I_h \rrbracket v_h^+ ds \right), \end{aligned} \quad (2.5)$$

$$l(v_h) = \sum_{K \in \mathcal{T}_h} \left( \int_K f_h v_h dx \right) - \sum_{K \in \mathcal{T}_h} \left( \int_{\partial_- K \cap \Gamma_h^-} (\Omega \cdot \mathbf{n}_h) g_h v_h^+ ds \right). \quad (2.6)$$

Here  $f_h = f \circ \Phi_h^{-1}$ ,  $g_h = \tilde{g} \circ \Phi_h^{-1}$ ,  $\tilde{g}$  is the zero extension of  $g$  on  $\Gamma$ . Note that  $\mathcal{B}(\cdot, \cdot)$  is the extension of the bilinear form defined for convex polyhedra in [16], now allowing  $F$  to be a curved face.

Employing integration by parts to (2.5) yields an alternative expression for the bilinear form

$$\begin{aligned} \mathcal{B}(I_h, v_h) &= \sum_{K \in \mathcal{T}_h} \left( \int_K (\sigma v_h - \Omega \cdot \nabla v_h) I_h dx \right) + \sum_{K \in \mathcal{T}_h} \left( \int_{\partial_+ K \cap \Gamma_h} (\Omega \cdot \mathbf{n}_h) I_h^+ v_h^+ ds \right) \\ &\quad + \sum_{K \in \mathcal{T}_h} \left( \int_{\partial_- K / \Gamma_h} (\Omega \cdot \mathbf{n}_h) \llbracket v_h \rrbracket I_h^- ds \right). \end{aligned} \quad (2.7)$$

Subsequently, the DG norm  $\|\cdot\|_{DG}$  can be defined by the average of (2.5) and (2.7)

$$\begin{aligned} \|v_h\|_{DG}^2 &= \sum_{K \in \mathcal{T}_h} \left( \int_K \sigma v_h^2 dx \right) + \frac{1}{2} \sum_{K \in \mathcal{T}_h} \left( \int_{\Gamma_h \cap \partial K} |\Omega \cdot \mathbf{n}_h| v_h^2 ds \right) \\ &\quad - \frac{1}{2} \sum_{K \in \mathcal{T}_h} \left( \int_{\partial_- K / \Gamma_h} \Omega \cdot \mathbf{n}_h \llbracket v_h \rrbracket^2 ds \right). \end{aligned}$$

Now we recall the stability of (2.4), which can be extended from Lemma 2.2 in [15] and Lemma 3.1 in [16].

**Lemma 2.1** *Assume that there exist two positive constants  $m$  and  $M$  such that  $0 < m \leq \sigma \leq M$ . Then the numerical solution  $I_h$  of (2.4) obeys the bound*

$$\begin{aligned} &\sum_{K \in \mathcal{T}_h} \left( \int_K \sigma I_h^2 dx + \int_{\partial_- K \cap \Gamma_h^-} |\Omega \cdot \mathbf{n}_h| I_h^2 ds + \int_{\partial_- K / \Gamma_h} |\Omega \cdot \mathbf{n}_h| \llbracket I_h \rrbracket^2 ds \right) \\ &\quad + \sum_{K \in \mathcal{T}_h} \left( \int_{\partial_+ K \cap \Gamma_h} \Omega \cdot \mathbf{n}_h I_h^2 ds \right) \lesssim \sum_{K \in \mathcal{T}_h} \left( \int_K f_h^2 dx + \int_{\partial_- K \cap \Gamma_h^-} g_h^2 ds \right). \end{aligned} \quad (2.8)$$

**Remark 1** *The Lemma 2.1 implies the uniqueness of the solution of the standard upwind DG method (2.4). Moreover, the existence of the solution  $I_h$  comes from its uniqueness because (2.4) is a linear problem over the finite-dimensional space  $V_{h,k}$ .*

### 3 Error analysis of the isoparametric finite element method

This section theoretically analyzes the error under the DG norm between the extension of the solution  $I$  in (1.1) and the numerical solution  $I_h$  of (2.4) on  $\mathcal{T}_h$ . To overcome the geometric inconsistency between the original domain  $D$  and its computational domain  $D_h$ , we extend the solution  $I$  in (1.1) to a function  $\tilde{I}$  defined on the hold-all region  $D_H = \text{convex}(D \cup D_h)$  [10], such that  $\tilde{I} \in H^{k+1}(\mathcal{T}_h) \cap W^{1,\infty}(\mathcal{T}_h)$ , and denote  $\tilde{f} = \Omega \cdot \nabla \tilde{I} + \sigma \tilde{I}$ . To characterize the effect of the geometric mapping, we define the transformed solution  $I^\dagger = I \circ \Phi_h^{-1}(x) \in H^1(D_H)$  [26]. It is noted that  $I^\dagger = g_h$  on the mapped boundary  $\Phi_h(\Gamma^-)$ .

#### 3.1 Approximation error in the isoparametric finite element space

Following the construction of the finite element space  $\hat{V}_{h,k}$ , which is equipped with the interpolation operator  $\hat{\Pi} : H^{k+1}(\hat{\mathcal{T}}_h) \rightarrow \hat{V}_{h,k}$  and the local  $L^2$  projection operator  $\hat{P} : L^2(\hat{\mathcal{T}}_h) \rightarrow \hat{V}_{h,k}$  [7], it is necessary to define a corresponding isoparametric auxiliary operator  $\Lambda : H^{k+1}(\mathcal{T}_h) \rightarrow V_{h,k}$ . For any  $v \in H^{k+1}(\mathcal{T}_h)$ , we denote  $\hat{v} = v \circ F_h \in H^{k+1}(\hat{\mathcal{T}}_h)$ . It is defined by

$$\Lambda v := (\hat{P}\hat{v}) \circ F_h^{-1} = [\hat{P}(v \circ F_h)] \circ F_h^{-1}. \quad (3.1)$$

In this subsection, we want to estimate the error  $\|\tilde{I} - \Lambda\tilde{I}\|_{DG}$  associated with the extension solution  $\tilde{I}$  and its approximation in  $V_{h,k}$ .

**Lemma 3.1** For  $\tilde{I} \in H^{k+1}(\mathcal{T}_h)$  and  $\Lambda : L^2(\mathcal{T}_h) \rightarrow V_{h,k}$ , there holds

$$\|\tilde{I} - \Lambda\tilde{I}\|_{DG} \lesssim h^{k+1/2} \|\tilde{I}\|_{H^{k+1}(\mathcal{T}_h)}. \quad (3.2)$$

**Proof. 1** Starting from the definition of  $\Lambda$ , employing the uniform boundedness of the geometric Jacobian  $\mathcal{J}_{F_h}$  and its inverse from assumption  $H_2$ , we derive

$$\begin{aligned} \|\tilde{I} - \Lambda\tilde{I}\|_{L^2(\mathcal{T}_h)} &= \|\tilde{I} - [\widehat{P}(\tilde{I} \circ F_h)] \circ F_h^{-1}\|_{L^2(\mathcal{T}_h)} \\ &= \|\mathcal{J}_{F_h}^{1/2}(\tilde{I} \circ F_h - \widehat{P}(\tilde{I} \circ F_h))\|_{L^2(\widehat{\mathcal{T}}_h)} \\ &= \|\mathcal{J}_{F_h}^{1/2}(\hat{I} - \widehat{P}\hat{I})\|_{L^2(\widehat{\mathcal{T}}_h)} \lesssim \|\hat{I} - \widehat{P}\hat{I}\|_{L^2(\widehat{\mathcal{T}}_h)} \\ &\lesssim h^{k+1} \|\hat{I}\|_{H^{k+1}(\widehat{\mathcal{T}}_h)} \lesssim h^{k+1} \|\tilde{I}\|_{H^{k+1}(\mathcal{T}_h)}. \end{aligned} \quad (3.3)$$

The penultimate inequality follows from the approximation property of the local  $L^2$  projection  $\widehat{P}$  on  $\widehat{V}_{h,k}$  [32], while the last inequality results from Eq.(2.2) and the assumption  $H_3$ .

Let  $\mathcal{E}_h = \{\bigcup \partial K : K \in \mathcal{T}_h\}$  and  $\widehat{\mathcal{E}}_h = \{\bigcup \partial \widehat{K} : \widehat{K} \in \widehat{\mathcal{T}}_h\}$  denote the sets of all element boundaries on  $\mathcal{T}_h$  and  $\widehat{\mathcal{T}}_h$ , respectively. Similar to (3.3) and invoking the trace theorem [7], we arrive at

$$\begin{aligned} &\| |\Omega \cdot \mathbf{n}_h|^{1/2} [\tilde{I} - \Lambda\tilde{I}] \|_{L^2(\mathcal{E}_h)} \\ &= \| |\Omega \cdot \mathbf{n}_h|^{1/2} [\tilde{I} - (\widehat{P}\hat{I}) \circ F_h^{-1}] \|_{L^2(\mathcal{E}_h)} \\ &= \| |\Omega \cdot \mathbb{B}_h \hat{\mathbf{n}}|^{1/2} [\hat{I} - \widehat{P}\hat{I}] \|_{L^2(\widehat{\mathcal{E}}_h)} \\ &\lesssim \| [\hat{I} - \widehat{P}\hat{I}] \|_{L^2(\widehat{\mathcal{E}}_h)} \lesssim h^{-1/2} \|\hat{I} - \widehat{P}\hat{I}\|_{H^{k+1}(\widehat{\mathcal{T}}_h)} \\ &\lesssim h^{k+1/2} \|\hat{I}\|_{H^{k+1}(\widehat{\mathcal{T}}_h)} \lesssim h^{k+1/2} \|\tilde{I}\|_{H^{k+1}(\mathcal{T}_h)}, \end{aligned} \quad (3.4)$$

where  $\mathbb{B}_h = \|\mathbb{J}_{F_h}^T \mathbf{n}_h\| \mathcal{J}_{F_h} \mathbb{J}_{F_h}^{-T}$  denotes the scaled Jacobian matrix, and  $\hat{\mathbf{n}} = \mathbb{J}_{F_h}^T \mathbf{n}_h / \|\mathbb{J}_{F_h}^T \mathbf{n}_h\|$  is the unit normal vector on  $\widehat{\mathcal{T}}_h$  [26].

Combining (3.3), (3.4) and the definition of the DG norm yields the estimates (3.2). The proof of Lemma 3.1 is completed.

**Lemma 3.2** Let  $\tilde{I}$  be the extension solution of (1.1) and let  $\Lambda : L^2(\mathcal{T}_h) \rightarrow V_{h,k}$  denote the isoparametric auxiliary operator. For any  $v_h \in V_{h,k}$  and the bilinear form  $\mathcal{B}(\cdot, \cdot)$  defined in (2.5), there holds

$$\mathcal{B}(\tilde{I} - \Lambda\tilde{I}, v_h) \lesssim \|\tilde{I} - \Lambda\tilde{I}\|_{DG} \|v_h\|_{DG}. \quad (3.5)$$

**Proof. 2** Utilizing the equivalent form of  $\mathcal{B}(\cdot, \cdot)$  in (2.7), we can decompose it into four parts

$$\begin{aligned} \mathcal{B}(\tilde{I} - \Lambda\tilde{I}, v_h) &= \sum_{K \in \mathcal{T}_h} \int_K \sigma v_h (\tilde{I} - \Lambda\tilde{I}) dx - \sum_{K \in \mathcal{T}_h} \int_K \Omega \cdot \nabla v_h (\tilde{I} - \Lambda\tilde{I}) dx \\ &\quad + \sum_{K \in \mathcal{T}_h} \int_{\partial_+ K \cap \Gamma_h} (\Omega \cdot \mathbf{n}_h) (\tilde{I} - \Lambda\tilde{I})^+ v_h^+ ds \\ &\quad + \sum_{K \in \mathcal{T}_h} \int_{\partial_- K / \Gamma_h} (\Omega \cdot \mathbf{n}_h) [v_h] (\tilde{I} - \Lambda\tilde{I})^- ds \\ &=: L_1 + L_2 + L_3 + L_4. \end{aligned} \quad (3.6)$$

From the definition of the DG norm, applying Cauchy-Schwarz inequality and the boundedness of  $\sigma$ , it is straightforward to observe that

$$L_1 + L_3 + L_4 \lesssim \|\tilde{I} - \Lambda\tilde{I}\|_{DG} \|v_h\|_{DG}.$$

For the term  $L_2$ , we employ the integral transformation  $F_h$  to arrive at

$$\begin{aligned} L_2 &= - \sum_{K \in \mathcal{T}_h} \int_K (\Omega \cdot \nabla v_h) [\tilde{I} - (\widehat{P}\hat{I}) \circ F_h^{-1}] dx \\ &= - \sum_{\widehat{K} \in \widehat{\mathcal{T}}_h} \int_{\widehat{K}} (\Omega \cdot \mathbb{J}_{F_h}^{-T} \nabla \hat{v}_h) (\hat{I} - \widehat{P}\hat{I}) \mathcal{J}_{F_h} d\hat{x} \end{aligned}$$

$$\begin{aligned}
&= - \sum_{\widehat{K} \in \widehat{\mathcal{T}}_h} \int_{\widehat{K}} \left[ \Omega \cdot (\mathbb{J}_{F_h}^{-T} - \mathbb{I}) \nabla \hat{v}_h \right] (\hat{I} - \widehat{P}\hat{I}) \mathcal{J}_{F_h} d\hat{x} \\
&\quad + \sum_{\widehat{K} \in \widehat{\mathcal{T}}_h} \int_{\widehat{K}} (\Omega \cdot \nabla \hat{v}_h) (\hat{I} - \widehat{P}\hat{I}) (1 - \mathcal{J}_{F_h}) d\hat{x} \\
&\quad - \sum_{\widehat{K} \in \widehat{\mathcal{T}}_h} \int_{\widehat{K}} (\Omega \cdot \nabla \hat{v}_h) (\hat{I} - \widehat{P}\hat{I}) d\hat{x} =: R_1 + R_2 + R_3.
\end{aligned} \tag{3.7}$$

From the assumptions  $H_2$  and  $H_3$ , it is clear to see

$$\|\mathbb{J}_{F_h}^{-T} - \mathbb{I}\|_{L^\infty(\widehat{D}_h)} \lesssim h, \quad \|1 - \mathcal{J}_{F_h}\|_{L^\infty(\widehat{D}_h)} \lesssim h, \quad \|\mathcal{J}_{F_h}\|_{L^\infty(\widehat{D}_h)} \lesssim 1.$$

Furthermore, by the inverse inequality of  $\widehat{V}_{h,k}$  [7], we can deduce

$$\begin{aligned}
R_1 + R_2 &\lesssim h \|\nabla \hat{v}_h\|_{L^2(\widehat{\mathcal{T}}_h)} \|\hat{I} - \widehat{P}\hat{I}\|_{L^2(\widehat{\mathcal{T}}_h)} \lesssim \|\hat{v}_h\|_{L^2(\widehat{\mathcal{T}}_h)} \|\hat{I} - \widehat{P}\hat{I}\|_{L^2(\widehat{\mathcal{T}}_h)} \\
&\lesssim \|v_h\|_{L^2(\mathcal{T}_h)} \|\tilde{I} - \Lambda\tilde{I}\|_{L^2(\mathcal{T}_h)}.
\end{aligned} \tag{3.8}$$

Finally, by the definition of local  $L^2$  projection onto  $\widehat{V}_{h,k}$ , we have  $R_3 = 0$ . The conclusion follows then from estimates (3.6), (3.7) and (3.8).

## 3.2 The consistency error of the upwind DG method

This subsection is devoted to estimating the consistency error  $\|\Lambda I - I_h\|_{DG}$ , which is closely linked to the discrete formulation (2.4). To properly deal with  $f_h$  and  $g_h$  in the linear form  $l(\cdot)$  in (2.6), the errors arising from solution extension and geometric approximation must be considered separately.

### 3.2.1 The difference between $\tilde{I}$ and $I^\dagger$

**Lemma 3.3** *Let  $\tilde{I}$  be the extension of exact solution  $I$ , and let  $I^\dagger = I \circ \Phi_h^{-1} \in H^1(\mathcal{T}_h)$  denote its transformed counterpart on the computational domain  $D_h$ . It holds that*

$$\|\tilde{I} - I^\dagger\|_{DG} \lesssim h^{k+\frac{1}{2}} \|\tilde{I}\|_{L^2(\mathcal{T}_h)} + h^{k+\frac{3}{2}} \|\tilde{I}\|_{H^2(\mathcal{T}_h)}. \tag{3.9}$$

**Proof. 3** *Employing the definition of  $I^\dagger$  and (2.2) yields*

$$\begin{aligned}
\|\tilde{I} - I^\dagger\|_{L^2(\mathcal{T}_h)}^2 &= \|\tilde{I} - I \circ \Phi_h^{-1}\|_{L^2(\mathcal{T}_h)}^2 = \|\tilde{I} - \tilde{I} \circ \Phi_h^{-1}\|_{L^2(\mathcal{T}_h)}^2 \\
&\leq \|\text{id} - \Phi_h^{-1}\|_{L^\infty(D_h)}^2 \|\tilde{I}\|_{L^2(\mathcal{T}_h)}^2 \leq h^{2k+2} \|\tilde{I}\|_{L^2(\mathcal{T}_h)}^2.
\end{aligned} \tag{3.10}$$

*Differentiating  $I^\dagger$  and applying the chain rule provides its gradient representation*

$$\nabla I^\dagger = \nabla(I \circ \Phi_h^{-1}) = \mathbb{J}_{\Phi_h}^{-T}(\nabla I) \circ \Phi_h^{-1} = \mathbb{J}_{\Phi_h}^{-T}(\nabla \tilde{I}) \circ \Phi_h^{-1}, \quad \text{in } D_h.$$

*Then it yields the gradient error estimate*

$$\begin{aligned}
\|\nabla \tilde{I} - \nabla I^\dagger\|_{L^2(\mathcal{T}_h)}^2 &= \|\nabla \tilde{I} - \mathbb{J}_{\Phi_h}^{-T}(\nabla \tilde{I}) \circ \Phi_h^{-1}\|_{L^2(\mathcal{T}_h)}^2 \\
&\leq \|(\mathbb{I} - \mathbb{J}_{\Phi_h}^{-T})\nabla \tilde{I}\|_{L^2(\mathcal{T}_h)}^2 + \|\mathbb{J}_{\Phi_h}^{-T}(\nabla \tilde{I} - \nabla \tilde{I} \circ \Phi_h^{-1})\|_{L^2(\mathcal{T}_h)}^2 \\
&\lesssim h^{2k} \|\tilde{I}\|_{H^1(\mathcal{T}_h)}^2 + h^{2k+2} \|\tilde{I}\|_{H^2(\mathcal{T}_h)}^2,
\end{aligned} \tag{3.11}$$

*where the first term reflects the auxiliary mapping approximation from (2.2) as well as the second term stems from the translation of the gradient field. Therefore, by the trace theorem and the estimations (3.10) and (3.11), the DG norm error satisfies*

$$\begin{aligned}
\|\tilde{I} - I^\dagger\|_{DG}^2 &\lesssim \|\tilde{I} - I^\dagger\|_{L^2(\mathcal{T}_h)}^2 + \|\tilde{I} - I^\dagger\|_{L^2(\varepsilon_h)}^2 \\
&\lesssim \|\tilde{I} - I^\dagger\|_{L^2(\mathcal{T}_h)}^2 + h^{-1} \|\tilde{I} - I^\dagger\|_{L^2(\mathcal{T}_h)}^2 + h \|\tilde{I} - I^\dagger\|_{H^1(\mathcal{T}_h)}^2 \\
&\lesssim h^{2k+1} \|\tilde{I}\|_{L^2(\mathcal{T}_h)}^2 + h^{2k+3} \|\tilde{I}\|_{H^2(\mathcal{T}_h)}^2.
\end{aligned} \tag{3.12}$$

*The proof of Lemma 3.3 is completed.*

### 3.2.2 Geometric approximation error of inflow boundary

The estimation of the geometric approximation error between the inflow boundary  $\Gamma_h^-$  of  $D_h$  and  $\Phi_h(\Gamma^-)$  relies on the following mild assumptions [13]

(A<sub>1</sub>)  $\Gamma_h$  is a compact, oriented, piecewise  $C^{k+1}$  smooth regular surface.

(A<sub>2</sub>) 0 is the regular value of the function  $f(x) = \Omega \cdot \mathbf{n}_h(x)$ , that is,  $\forall x \in f^{-1}(0)$ ,  $\nabla f(x) \neq 0$ .

**Lemma 3.4** *Suppose that the assumptions A<sub>1</sub> and A<sub>2</sub> hold, and let  $h > 0$  be sufficiently small. Then the area of the set  $T_{h^k} = \{x \in \Gamma_h : |\Omega \cdot \mathbf{n}_h(x)| \lesssim h^k\}$  satisfies*

$$\text{Area}(T_{h^k}) \lesssim h^k. \quad (3.13)$$

**Proof. 4** *Let  $\mathcal{E}_h^c$  denote the collection of all curved boundary faces constituting  $\Gamma_h$ . For each face  $F \in \mathcal{E}_h^c$ , the restricted function  $f|_F = \Omega \cdot \mathbf{n}_h|_F$  belongs to  $C^k(F)$ . By assumption (A<sub>2</sub>), 0 is a regular value of  $f|_F$ . Consequently, the zero level set  $\Gamma_F^0 := f|_F^{-1}(0)$ , when non-empty, is a finite union of  $C^1$  one-dimensional submanifolds in  $F$ .*

*We now focus on faces where  $\Gamma_F^0$  is non-empty. Applying the methodology of geometric measure theory [13], the regularity condition  $\nabla f \neq 0$  on  $\Gamma_F^0$  guarantees the existence of a local tubular neighborhood. Within this neighborhood, we can construct coordinates  $(s, r)$  where  $s$  parametrizes  $\Gamma_F^0$  and the normal coordinate  $r$  satisfies the key equivalence*

$$c_1|r| \leq |f(x)| \leq c_2|r|, \quad \text{and} \quad |r| \approx \text{dist}(x, \Gamma_F^0),$$

*for positive constants  $c_1, c_2$  independent of  $h$  and the face  $F$ . It follows directly that*

$$F_* := T_{h^k} \cap F \subset \{x : |r(x)| \lesssim h^k\}.$$

*The face  $F$  in  $(s, r)$ -coordinates takes the form  $dS = J(s, r)dsdr$ , with  $J(s, 0) = 1$  and  $|J(s, r) - 1| \lesssim |r|$  due to the smoothness of  $F$ . Integrating over the tubular neighborhood  $F_*$  yields the local estimate*

$$\text{Area}(T_{h^k} \cap F) \lesssim \text{Length}(\Gamma_F^0 \cap F) \cdot h^k. \quad (3.14)$$

*The final estimate follows by summing over all boundary faces  $\mathcal{E}_h^c$ . Under the shape-regularity and quasi-uniformity of  $\mathcal{T}_h$ , the total length of the discrete zero level set remains bounded independently of  $h$*

$$\sum_{F \in \mathcal{F}_h} \text{Length}(\Gamma_F^0) \lesssim 1.$$

*Summing the local estimates (3.14), we obtain*

$$\text{Area}(T_{h^k}) = \sum_{F \in \mathcal{F}_h} \text{Area}(T_{h^k} \cap F) \lesssim \left( \sum_{F \in \mathcal{F}_h} \text{Length}(\Gamma_F^0 \cap F) \right) h^k \lesssim h^k. \quad (3.15)$$

*The proof of Lemma 3.4 is completed.*

**Lemma 3.5** *Let  $A \Delta B$  denote the symmetric difference of two sets  $A$  and  $B$ . Suppose  $\Gamma^-$  and  $\Gamma_h^-$  are the inflow boundaries of  $D$  and  $D_h$ , respectively. Then, the area of symmetric difference under the mapping  $\Phi_h$  satisfies*

$$\text{Area}(\Gamma_h^- \Delta \Phi_h(\Gamma^-)) \lesssim h^k. \quad (3.16)$$

**Proof. 5** *The relation between the unit outward normal vectors  $\mathbf{n}$  on  $\Gamma$  and  $\mathbf{n}_h$  on  $\Gamma_h$  is given by  $\mathbf{n}_h(x) = \mathbb{J}_{\Phi_h}^{-T} \mathbf{n} / \|\mathbb{J}_{\Phi_h}^{-T} \mathbf{n}\|$ . Let  $\mathbf{n}_s = \mathbf{n} / \|\mathbb{J}_{\Phi_h}^{-T} \mathbf{n}\|$  denote the scaled normal on  $\Gamma$ . Applying the mapping estimate (2.2) and Proposition 2 in [23], we observe*

$$\begin{aligned} \|\mathbf{n}_s \circ \Phi_h^{-1} - \mathbf{n}_h\|_{L^\infty(\Gamma_h)} &= \|\mathbb{J}_{\Phi_h}^T \mathbf{n}_s - \mathbf{n}_h\|_{L^\infty(\Gamma_h)} \\ &= \|(\mathbb{J}_{\Phi_h}^T - \mathbb{I})\mathbf{n}_s\|_{L^\infty(\Gamma_h)} \lesssim h^k. \end{aligned} \quad (3.17)$$

Consequently

$$|\Omega \cdot \mathbf{n}_s \circ \Phi_h^{-1}(x) - \Omega \cdot \mathbf{n}_h(x)| \lesssim h^k, \forall x \in \Gamma_h. \quad (3.18)$$

Recall the definitions of the inflow boundaries

$$\Gamma^- = \{x \in \Gamma : \Omega \cdot \mathbf{n}(x) < 0\}, \Gamma_h^- = \{x \in \Gamma_h : \Omega \cdot \mathbf{n}_h(x) < 0\}.$$

Consider a point  $x \in \Gamma_h^- / \Phi_h(\Gamma^-)$ . Since  $x \notin \Phi_h(\Gamma^-)$ , we have  $\Phi_h^{-1}(x) \notin \Gamma^-$ , which implies  $\Omega \cdot \mathbf{n}_s \circ \Phi_h^{-1}(x) \geq 0$ . A symmetric argument applies to a point  $x \in \Phi_h(\Gamma^-) / \Gamma_h^-$ . It follows that the difference region between  $\Gamma_h^-$  and  $\Phi_h(\Gamma^-)$  can be controlled by the  $h^k$  tube of  $f(x) = \Omega \cdot \mathbf{n}_h(x)$ , that is

$$T_{h^k} = \{x \in \Gamma_h, |f(x)| \lesssim h^k\}. \quad (3.19)$$

After combining (3.19) and the Lemma 3.4, the proof of (3.16) is completed.

**Remark 2** While Lemma 3.5 shares a similar form to Eq. (3.9) in [8], its focus and dependence are different. Lemma 3.5 specifically estimates the discrepancy between inflow boundary  $\Gamma_h^-$  and isoparametrically mapped counterpart  $\Phi_h(\Gamma^-)$ , an estimate that depends explicitly on the mapping  $\Phi_h$  and the unit normal vector  $\mathbf{n}_h$ . In contrast, the results in [8] concern estimates that depend only on the auxiliary mapping, without involving the boundary normal explicitly.

**Lemma 3.6** Let  $\mathcal{E}_h^0$  be the set of boundary faces adjacent to  $\Gamma_h^0 := \{x \in \Gamma_h : \Omega \cdot \mathbf{n}_h(x) = 0\}$ . For any  $x \in \mathcal{E}_h^0$ , there holds

$$|\Omega \cdot \mathbf{n}_h(x)| \lesssim h \|\mathbf{n}_h\|_{W^{1,\infty}(\mathcal{E}_h^0)}. \quad (3.20)$$

Furthermore, for  $x \in \Gamma_h^- \Delta \Phi_h(\Gamma^-)$ , it follows that

$$|\Omega \cdot \mathbf{n}_h(x)| \lesssim h^k \|\mathbf{n}_h\|_{W^{1,\infty}(\Gamma_h)}. \quad (3.21)$$

**Proof. 6** For any  $x \in \mathcal{E}_h^0$ , there exists  $x_0 \in \overline{\mathcal{E}_h^0} \cap \Gamma_h^0$  with  $\Omega \cdot \mathbf{n}_h(x_0) = 0$ . Since  $|x - x_0| \lesssim h$  and  $\Omega \cdot \mathbf{n}_h$  is Lipschitz on  $\mathcal{E}_h^0$ , it follows that

$$|\Omega \cdot \mathbf{n}_h(x)| = |\Omega \cdot \mathbf{n}_h(x) - \Omega \cdot \mathbf{n}_h(x_0)| \leq h \|\mathbf{n}_h\|_{W^{1,\infty}(\mathcal{E}_h^0)}, \forall x \in \mathcal{E}_h^0. \quad (3.22)$$

Lemma 3.5 implies that any  $x \in \Gamma_h^- \Delta \Phi_h(\Gamma^-)$  satisfies  $\text{dist}(x, \Gamma_h^0) \lesssim h^k$ . Choosing  $x_0 \in \Gamma_h^0$  with  $|x - x_0| \lesssim h^k$  and similar to (3.22), we arrive at

$$|\Omega \cdot \mathbf{n}_h(x)| = |\Omega \cdot \mathbf{n}_h(x) - \Omega \cdot \mathbf{n}_h(x_0)| \lesssim h^k \|\mathbf{n}_h\|_{W^{1,\infty}(\Gamma_h)}, \forall x \in \Gamma_h^- \Delta \Phi_h(\Gamma^-). \quad (3.23)$$

The conclusions follow from the estimates (3.22) and (3.23).

**Theorem 3.7** Let  $I$  be the solution of (1.1), and  $\tilde{I} \in H^{k+1}(\mathcal{T}_h) \cap W^{1,\infty}(\mathcal{T}_h)$  denotes its regular extension to the computational domain. Let  $f_h \in W^{1,\infty}(\mathcal{T}_h)$  and  $I_h$  be the numerical solution of (2.4). Suppose that the assumptions ( $H_1 \sim H_3$ ) and ( $A_1 \sim A_2$ ) hold. Then for any  $k \geq 2$ , there holds

$$\|\tilde{I} - I_h\|_{DG} \lesssim h^{k+\frac{1}{2}} \left( \|f_h\|_{W^{1,\infty}(\mathcal{T}_h)} + \|\tilde{I}\|_{H^{k+1}(\mathcal{T}_h)} + \|\tilde{I}\|_{W^{1,\infty}(\mathcal{T}_h)} \right). \quad (3.24)$$

**Proof. 7** Applying the triangle inequality and Lemma 3.2, we decompose the DG error between  $\tilde{I}$  and  $I_h$  into two parts

$$\begin{aligned} \|\tilde{I} - I_h\|_{DG} &\leq \|\tilde{I} - \Lambda\tilde{I}\|_{DG} + \|\Lambda\tilde{I} - I_h\|_{DG} \\ &= \|\tilde{I} - \Lambda\tilde{I}\|_{DG} + \frac{\mathcal{B}(\Lambda\tilde{I} - I_h, \Lambda\tilde{I} - I_h)}{\|\Lambda\tilde{I} - I_h\|_{DG}} \\ &\lesssim \|\tilde{I} - \Lambda\tilde{I}\|_{DG} + \frac{\mathcal{B}(\tilde{I} - I_h, \Lambda\tilde{I} - I_h)}{\|\Lambda\tilde{I} - I_h\|_{DG}} \\ &=: L_1 + L_2. \end{aligned} \quad (3.25)$$

The term  $L_1$  is directly bounded by Lemma 3.1, and we only consider  $L_2$ . We express the bilinear form (2.5) acting on the extended solution  $\tilde{I}$ . Utilizing the definition of  $\tilde{f}$  in Section 3 and the continuity of  $\tilde{I}$  across interior faces yield

$$\begin{aligned}
& \mathcal{B}(\tilde{I}, v_h) \\
&= \sum_{K \in \mathcal{T}_h} \left( \int_K (\Omega \cdot \nabla \tilde{I} + \sigma \tilde{I}) v_h dx \right) - \sum_{K \in \mathcal{T}_h} \left( \int_{\partial_- K \cap \Gamma_h^-} (\Omega \cdot \mathbf{n}_h) \tilde{I} v_h ds \right) \\
&\quad - \sum_{K \in \mathcal{T}_h} \left( \int_{\partial_- K / \Gamma_h} (\Omega \cdot \mathbf{n}_h) [\tilde{I}] v_h^+ ds \right) \\
&= \sum_{K \in \mathcal{T}_h} \left( \int_K \tilde{f} v_h dx \right) - \sum_{K \in \mathcal{T}_h} \left( \int_{\partial_- K \cap \Gamma_h^-} (\Omega \cdot \mathbf{n}_h) \tilde{I} v_h ds \right). \tag{3.26}
\end{aligned}$$

Then recalling the discrete problem (2.4) and the property  $\tilde{f} = f$  in  $D_h$ , we observe

$$\begin{aligned}
& \mathcal{B}(I_h, v_h) = l(v_h) \\
&= \sum_{K \in \mathcal{T}_h} \left( \int_K f_h v_h dx \right) - \sum_{K \in \mathcal{T}_h} \left( \int_{\partial_- K \cap \Gamma_h^-} (\Omega \cdot \mathbf{n}_h) g_h v_h ds \right) \\
&= \sum_{K \in \mathcal{T}_h} \left( \int_K f \circ \Phi_h^{-1} v_h dx \right) - \sum_{K \in \mathcal{T}_h} \left( \int_{\partial_- K \cap \Gamma_h^-} (\Omega \cdot \mathbf{n}_h) g_h v_h ds \right) \\
&= \sum_{K \in \mathcal{T}_h} \left( \int_K \tilde{f} \circ \Phi_h^{-1} v_h dx \right) - \sum_{K \in \mathcal{T}_h} \left( \int_{\partial_- K \cap \Gamma_h^-} (\Omega \cdot \mathbf{n}_h) g_h v_h ds \right). \tag{3.27}
\end{aligned}$$

Combining (3.26) and (3.27), we arrive at

$$\begin{aligned}
& \mathcal{B}(\tilde{I} - I_h, v_h) = \sum_{K \in \mathcal{T}_h} \left( \int_K (\tilde{f} - \tilde{f} \circ \Phi_h^{-1}) v_h dx \right) \\
&\quad + \sum_{K \in \mathcal{T}_h} \left( \int_{\partial_- K \cap \Gamma_h^-} (\Omega \cdot \mathbf{n}_h) g_h v_h ds - \int_{\partial_- K \cap \Gamma_h^-} (\Omega \cdot \mathbf{n}_h) \tilde{I} v_h ds \right) \\
&=: E_1 + E_2, \tag{3.28}
\end{aligned}$$

where

$$E_1 = \sum_{K \in \mathcal{T}_h} \left( \int_K (\tilde{f} - \tilde{f} \circ \Phi_h^{-1}) v_h dx \right) \leq h^{k+1} \|\tilde{f}\|_{W^{1,\infty}(\mathcal{T}_h)} \|v_h\|_{DG}. \tag{3.29}$$

For the term  $E_2$ , we note

$$g_h = \tilde{g} \circ \Phi_h^{-1} = g \circ \Phi_h^{-1} = I \circ \Phi_h^{-1} = I^\dagger, \quad \text{on } \Phi_h(\Gamma^-).$$

Consequently, it can be decomposed into three parts

$$\begin{aligned}
E_2 &= \sum_{K \in \mathcal{T}_h} \left( \int_{\partial_- K \cap \Gamma_h^-} (\Omega \cdot \mathbf{n}_h) g_h v_h ds - \int_{\partial_- K \cap \Gamma_h^-} (\Omega \cdot \mathbf{n}_h) \tilde{I} v_h ds \right) \\
&= \sum_{K \in \mathcal{T}_h} \left( \int_{\partial_- K \cap (\Gamma_h^- \cap \Phi_h(\Gamma^-))} (\Omega \cdot \mathbf{n}_h) (I^\dagger - \tilde{I}) v_h ds \right) \\
&\quad + \sum_{K \in \mathcal{T}_h} \left( \int_{\partial_- K \cap (\Gamma_h^- / \Phi_h(\Gamma^-))} (\Omega \cdot \mathbf{n}_h) g_h v_h ds \right) \\
&\quad - \sum_{K \in \mathcal{T}_h} \left( \int_{\partial_- K \cap (\Gamma_h^- / \Phi_h(\Gamma^-))} (\Omega \cdot \mathbf{n}_h) \tilde{I} v_h ds \right) \\
&=: T_1 + T_2 + T_3. \tag{3.30}
\end{aligned}$$

From Lemma 3.3, we directly get the bound  $T_1 \lesssim h^{k+\frac{1}{2}} \|\tilde{I}\|_{L^2(\mathcal{T}_h)}$ . Moreover, since  $g_h = \tilde{g} \circ \Phi_h^{-1}$  and  $\tilde{g}$  is the zero extension on  $\Gamma$ , it follows that  $T_2 = 0$ .

For the term  $T_3$ , let  $D_c$  denote the set of boundary elements intersected by the characteristic boundary  $\Gamma_h^0$ , which means  $D_c = \{K \in \mathcal{T}_h : \partial K \cap \Gamma^0 \neq \emptyset\}$ . By (3.9),  $D_c$  satisfies  $\text{Vol}(D_c) \lesssim h^{k+1}$  according to (3.9). Utilizing the estimates (2.3), Cauchy-Schwarz inequality and Lemma 3.6, we accept the fact

$$\begin{aligned}
T_3 &= - \sum_{K \in \mathcal{T}_h} \left( \int_{\partial_- K \cap (\Gamma_h^- / \Phi_h(\Gamma^-))} (\Omega \cdot \mathbf{n}_h) \tilde{I} v_h ds \right) \tag{3.31} \\
&\lesssim h^k \sum_{K \in \mathcal{T}_h} \|\tilde{I}\|_{L^2(\partial_- K \cap (\Gamma_h^- / \Phi_h(\Gamma^-))} \|v_h\|_{L^2(\partial_- K \cap (\Gamma_h^- / \Phi_h(\Gamma^-))} \\
&\lesssim h^k \left( \sum_{K \in \mathcal{T}_h} \|\tilde{I}\|_{L^2(\partial_- K \cap (\Gamma_h^- / \Phi_h(\Gamma^-))}^2 \right)^{\frac{1}{2}} \left( \sum_{K \in \mathcal{T}_h} \|v_h\|_{L^2(\partial_- K \cap (\Gamma_h^- / \Phi_h(\Gamma^-))}^2 \right)^{\frac{1}{2}} \\
&\lesssim h^k \left( \sum_{K \in D_c} \left\{ h_K^{-1} \|\tilde{I}\|_{L^2(K)}^2 + h_K \|\tilde{I}\|_{H^1(K)}^2 \right\} \right)^{\frac{1}{2}} \\
&\quad \cdot \left( \sum_{K \in D_c} \left\{ h_K^{-1} \|v_h\|_{L^2(K)}^2 + h_K \|v_h\|_{H^1(K)}^2 \right\} \right)^{\frac{1}{2}} \\
&\lesssim h^k \cdot h^{-\frac{1}{2}} \text{Vol}(D_c)^{\frac{1}{2}} \cdot \|\tilde{I}\|_{W^{1,\infty}(\mathcal{T}_h)} \cdot h^{-\frac{1}{2}} \|v_h\|_{DG} \\
&\lesssim h^k \cdot h^{\frac{k-1}{2}} \|\tilde{I}\|_{W^{1,\infty}(\mathcal{T}_h)} \|v_h\|_{DG} \lesssim h^{k+\frac{1}{2}} \|\tilde{I}\|_{W^{1,\infty}(\mathcal{T}_h)} \|v_h\|_{DG}. \tag{3.32}
\end{aligned}$$

Collecting the results (3.2), (3.9), (3.29) and (3.31), we finally obtain the estimate (3.24). The proof of Theorem 3.7 is completed.

## 4 Numerical Experiment

In this section, we carry out numerical experiments on curved domains to verify the theoretical results. These experiments are conducted by employing the open-source finite element software package NUDG++ [14] for 2D case and the adaptive finite element package Parallel Hierarchical Grid (PHG) [36] for 3D case.

### 4.1 Example two-dimensional(2D)

To construct a representative test case, we make the following specific choices. For the RTE with the absorption coefficient  $\sigma = 1$ , the discrete direction is set to the unit vector  $\Omega = (\frac{\sqrt{3}}{2}, \frac{1}{2})^T$ , the exact solution is taken as  $I(x, y) = \sin(\pi x + \pi y) + x^2 + y^2 + xy + 5$ , and the original domain is the curved disc defined by

$$D = \{(x, y) : x^2 + y^2 < 0.25\}.$$

The 2D straight mesh  $\mathcal{T}_{h_1} \sim \mathcal{T}_{h_6}$  are generated by Gmsh with global mesh size factor 2, 1, 0.5, 0.25, 0.125 and 0.0625, receptively. Moreover, utilizing the approximation  $h_i \propto \text{N dof}_i^{-\frac{1}{2}}$  ( $i = 1, 2, \dots, 6$ ), where  $\text{N dof}_i$  is the number of Degree of Freedom(DOF), we could estimate the error convergence rate by

$$\text{rate}_i = \frac{\ln(\text{error}_i / \text{error}_{i-1})}{\ln(h_i / h_{i-1})}, \quad i = 2, \dots, 6. \tag{4.1}$$

As shown in Table 1, the error convergence rates under the DG norms agree perfectly with the Theorem 3.7 for  $k = 2$  and  $k = 3$ .

### 4.2 Example three-dimensional(3D)

For 3D case, we conduct a series of comparative experiments on  $\widehat{\mathcal{T}}_h$  and  $\mathcal{T}_h$  to demonstrate the advantages of computation on curved domains. For brevity, we select the absorption coefficient

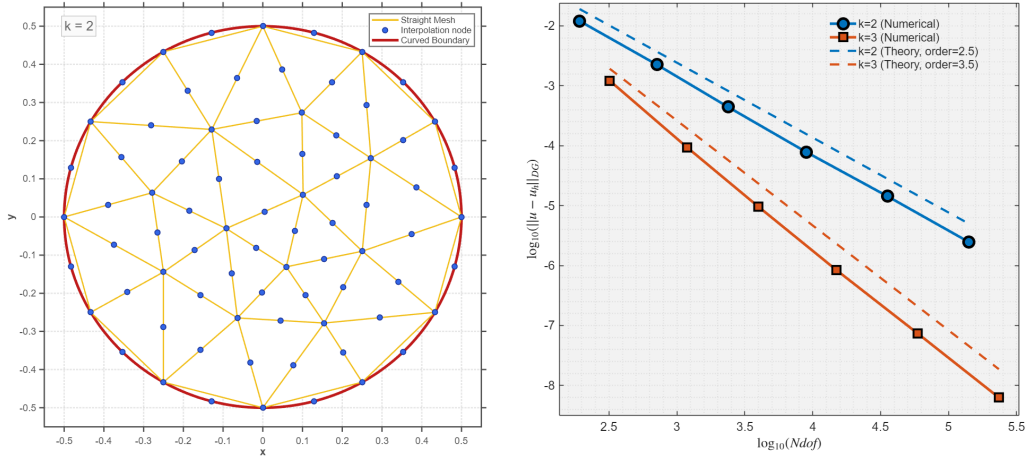


Figure 1: Isoparametric mapping and numerical results in 2D. Left: The straight mesh  $\widehat{\mathcal{T}}_{h_1}$  (yellow), interpolation nodes (blue), and curved domain boundary (red) after isoparametric mapping with  $k = 2$ . Right: Numerical and theoretical convergence rate on  $\mathcal{T}_h$  for  $k = 2$  and  $k = 3$ .

Table 1: Convergence rate on mesh  $\mathcal{T}_h$  of unit circle with  $k = 2$  &  $k = 3$

$k$	Mesh	Nelem	Ndof	$L^2$ error	$L^2$ rate	DG error	DG rate
2	$\mathcal{T}_{h_1}$	32	192	3.3747e-03	-	1.2060e-02	-
	$\mathcal{T}_{h_2}$	119	714	4.5822e-04	3.0405	2.2467e-03	2.5589
	$\mathcal{T}_{h_3}$	397	2382	6.1777e-05	3.3264	4.4307e-04	2.6950
	$\mathcal{T}_{h_4}$	1497	8982	7.9332e-06	3.0927	7.8135e-05	2.6148
	$\mathcal{T}_{h_5}$	5908	35448	1.0275e-06	2.9776	1.4367e-05	2.4672
	$\mathcal{T}_{h_6}$	23452	140712	1.3519e-07	2.9424	2.4791e-06	2.5489
3	$\mathcal{T}_{h_1}$	32	320	2.7108e-04	-	1.2164e-03	-
	$\mathcal{T}_{h_2}$	119	1190	1.5649e-05	4.3429	9.3544e-05	3.9062
	$\mathcal{T}_{h_3}$	397	3970	1.1180e-06	4.3806	9.6579e-06	3.7693
	$\mathcal{T}_{h_4}$	1497	14970	7.0975e-08	4.1543	8.3750e-07	3.6844
	$\mathcal{T}_{h_5}$	5908	59080	4.5273e-09	4.0095	7.4028e-08	3.5342
	$\mathcal{T}_{h_6}$	23452	234520	2.9106e-10	3.9812	6.2822e-09	3.5785

$\sigma = 1$ , the discrete direction  $\Omega = \left(\frac{1}{\sqrt{3}}, \frac{1}{\sqrt{3}}, \frac{1}{\sqrt{3}}\right)^T$ , the exact solution  $I(x, y, z) = \sin(\pi x + \pi y + \pi z) + x^2 + y^2 + z^2 + xyz + 5$  and the original domain is taken as the curved region defined by

$$D = \{(x, y, z) : x^2 + y^2 + z^2 < 1\}.$$

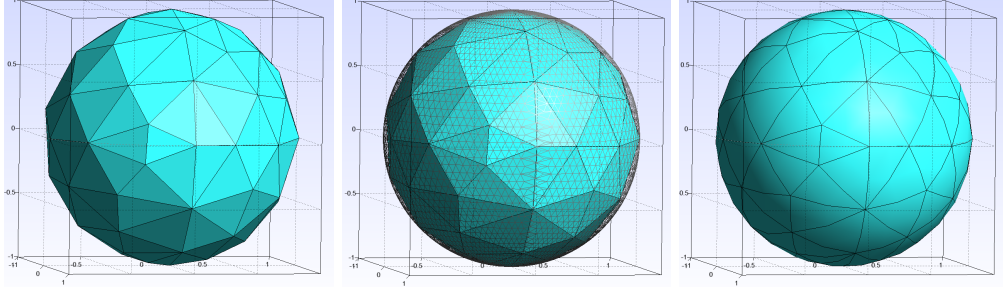


Figure 2: Mesh and domain evolution through isoparametric mapping in 3D. Left: The straight mesh  $\widehat{\mathcal{T}}_h$  with convex polyhedron domain  $\widehat{D}_h$ . Middle: The straight mesh  $\widehat{\mathcal{T}}_h$  (light blue) with curved domain  $D_h$  (gray). Right: The curved mesh  $\mathcal{T}_h$  with curved domain  $D_h$ .

In the actual calculation, we transform the integrals of curved elements  $K \in \mathcal{T}_h$  and surface integrals to those of straight elements  $\widehat{K} \in \widehat{\mathcal{T}}_h$  for calculation [26]

$$\int_K f d\mathbf{x} = \int_{\widehat{K}} \widehat{f} \mathcal{J}_{F_h(x)} d\widehat{\mathbf{x}}, \quad \int_F f d\mathbf{s} = \int_{\widehat{F}} \widehat{f} \mathcal{J}_{F_h(\widehat{x})} \|\mathbb{J}_{F_h(\widehat{x})}^{-T} \widehat{\mathbf{n}}\| d\widehat{\mathbf{s}}. \quad (4.2)$$

where  $\mathbb{J}_{F_h(\widehat{x})}$  and  $\mathcal{J}_{F_h(x)}$  are the Jacobian matrix and its determinant of  $F_h$ ,  $\widehat{\mathbf{n}}$  is the unit outer normal of  $\widehat{F}$ . Moreover, employing the approximation  $h_i \propto N_i^{-\frac{1}{3}}$  ( $i = 1, 2, \dots, 6$ ), we also use the formula (4.1) to compute the convergence rate.

Table 2: Convergence rate on straight mesh  $\widehat{\mathcal{T}}_h$  of convex polyhedron domain  $\widehat{D}_h$  with  $k = 2$

Mesh	Nelem	Ndof	$L^2$ error	$L^2$ rate	DG error	DG rate
$\widehat{\mathcal{T}}_{h_1}$	48	480	3.4686e-01	-	5.0478e-01	-
$\widehat{\mathcal{T}}_{h_2}$	384	3840	1.2340e-01	1.4910	2.0939e-01	1.2695
$\widehat{\mathcal{T}}_{h_3}$	3072	30720	1.5694e-02	2.9751	4.7381e-02	2.1438
$\widehat{\mathcal{T}}_{h_4}$	24576	245760	1.6289e-03	3.2682	8.5384e-03	2.4723
$\widehat{\mathcal{T}}_{h_5}$	196608	1966080	1.9103e-04	3.0920	1.5069e-03	2.5024

The straight mesh  $\widehat{\mathcal{T}}_{h_1}$  in Table 2 and Table 3 is generated by Netgen,  $\widehat{\mathcal{T}}_{h_2} \sim \widehat{\mathcal{T}}_{h_5}$  are derived from the command `phgRefineAllElements` with  $\widehat{\mathcal{T}}_{h_1}$ . The curved mesh  $\mathcal{T}_{h_i}$  in Table 4 is derived from  $\widehat{\mathcal{T}}_{h_i}$  ( $i = 1, 2, \dots, 6$ ) by the isoparametric mapping  $F_h$ .

We compare the convergence rates for different mesh-domain configurations in Table 2 and Table 3. While a straight mesh  $\widehat{\mathcal{T}}_h$  on a convex polyhedron domain  $\widehat{D}_h$  yields optimal convergence in both the  $L^2$  and DG norms [7, 10, 29], applying the same mesh to corresponding curved domain  $D_h$  results in degraded performance. The inaccuracy of the straight mesh in capturing the boundary geometry leads to the dominance of the geometric approximation error [11].

The results in Table 4 illustrate the optimal convergence rate in the DG norm achieved by a curved mesh  $\mathcal{T}_h$  on a curved domain  $D_h$ , which confirms the Theorem 3.7. This success demonstrates that isoparametric elements by high-order methods are essential for achieving the optimal accuracy on curved domains.

Table 3: Convergence rate on straight mesh  $\widehat{\mathcal{T}}_h$  of curved domain  $D_h$  with  $k = 2$ 

Mesh	Nelem	Ndof	$L^2$ error	$L^2$ rate	DG error	DG rate
$\widehat{\mathcal{T}}_{h_1}$	48	480	4.8805e-01	-	7.0139e-01	-
$\widehat{\mathcal{T}}_{h_2}$	384	3840	1.6281e-01	1.5838	2.7039e-01	1.3752
$\widehat{\mathcal{T}}_{h_3}$	3072	30720	2.8623e-02	2.5079	6.2308e-02	2.1176
$\widehat{\mathcal{T}}_{h_4}$	24576	245760	6.2782e-03	2.1888	1.3013e-02	2.2595
$\widehat{\mathcal{T}}_{h_5}$	196608	1966080	1.5401e-03	2.0273	2.8423e-03	2.1948

Table 4: Convergence rate on curved mesh  $\mathcal{T}_h$  of curved domain  $D_h$  with  $k = 2$ 

Mesh	Nelem	Ndof	$L^2$ error	$L^2$ rate	DG error	DG rate
$\mathcal{T}_{h_1}$	48	480	2.5781e-01	-	7.3825e-01	-
$\mathcal{T}_{h_2}$	384	3840	6.4164e-02	2.0065	2.0012e-01	1.8832
$\mathcal{T}_{h_3}$	3072	30720	1.2140e-02	2.4020	4.5983e-02	2.1217
$\mathcal{T}_{h_4}$	24576	245760	1.5993e-03	2.9243	8.5462e-03	2.4277
$\mathcal{T}_{h_5}$	196608	1966080	1.9688e-04	3.0221	1.5123e-03	2.4985

## 5 Conclusion

We have presented a rigorous error analysis for the isoparametric upwind DG method applied to the RTE on curved domains. By estimating the approximation error of the isoparametric finite element space and the consistency error of the upwind DG scheme, we derived an optimal convergence rate of  $\mathcal{O}(h^{k+\frac{1}{2}})$  in the DG norm. This result balances the geometric approximation error and the numerical discretization error. Two-dimensional numerical experiments confirmed the theoretical predictions for  $k = 2$  and  $k = 3$ . Furthermore, three-dimensional examples demonstrated the advantages of isoparametric elements for high-order methods on curved domains. The analysis and numerical results establish the efficacy of the proposed approach for problems involving curved geometries.

**Funding** Lingxiao Li was supported by the National Key R&D Program of China under Grant 2023YFA1011000 and the NSF of China under Grant 12571385. Changhui Yao was supported by the NSF of China under Grant 12571394, the NSF of Henan Province under Grant 252300423016 and the KSRP in Universities of Henan Province under Grant 26A110019.

## References

- [1] Andreev, A. B., & Todorov, T. D.: Isoparametric finite element approximation for a boundary flux problem. *Int. J. Numer. Methods Heat Fluid Flow*, 16(1), 46-66 (2006)
- [2] Arnold, D. N., & Walker, S. W.: The Hellan–Herrmann–Johnson method with curved elements. *SIAM J. Numer. Anal.*, 58(5), 2829-2855 (2020)
- [3] Aylwin, R., & Jerez-Hanckes, C.: Finite-element domain approximation for Maxwell variational problems on curved domains. *SIAM J. Numer. Anal.*, 61(3), 1139-1171 (2023)
- [4] Bertrand, F., Munzenmaier, S., & Starke, G. First-order system least squares on curved boundaries: Higher-order Raviart–Thomas elements. *SIAM J. Numer. Anal.*, 52(6), 3165-3180 (2014)
- [5] Bertrand, F., & Starke, G.: Parametric Raviart–Thomas elements for mixed methods on domains with curved surfaces. *SIAM J. Numer. Anal.*, 54(6), 3648-3667 (2016).

- [6] Bramble, J. H., & King, J. T.: A robust finite element method for nonhomogeneous Dirichlet problems in domains with curved boundaries. *Math. Comp.*, 63(207), 1-17 (1994)
- [7] Brenner, S. C., & Scott, L. R.: *The mathematical theory of finite element methods*. New York, NY: Springer New York (2008)
- [8] Brenner, S. C., Neilan, M., & Sung, L. Y.: Isoparametric  $C^0$  interior penalty methods for plate bending problems on smooth domains. *Calcolo*, 50(1), 35-67 (2013)
- [9] Brezzi, F., Marini, L. D., & Süli, E.: Discontinuous Galerkin methods for first-order hyperbolic problems. *Math. Models Methods Appl. Sci.*, 14(12), 1893-1903 (2004)
- [10] Ciarlet, P. G., & Raviart, P. A.: *The combined effect of curved boundaries and numerical integration in isoparametric finite element methods*. Academic Press (1972)
- [11] Ciarlet, P. G.: *The finite element method for elliptic problems*. Society for Industrial and Applied Mathematics (2002)
- [12] Cockburn, B., Dong, B., & Guzman, J.: Optimal convergence of the original DG method for the transport-reaction equation on special meshes. *SIAM J. Numer. Anal.*, 46(3), 1250-1265 (2008)
- [13] Federer, H.: *Geometric measure theory*. Springer (2014)
- [14] Hesthaven, J. S., & Warburton, T.: *Nodal discontinuous Galerkin methods: algorithms, analysis, and applications*. New York, NY: Springer New York (2008)
- [15] Houston, P., Schwab, C., & Süli, E.: Stabilized hp-finite element methods for first-order hyperbolic problems. *SIAM J. Numer. Anal.*, 37(5), 1618-1643 (2000)
- [16] Houston, P., Schwab, C., & Süli, E.: Discontinuous hp-finite element methods for advection-diffusion-reaction problems. *SIAM J. Numer. Anal.*, 39(6), 2133-2163 (2002)
- [17] Hughes, T. J., Cottrell, J. A., & Bazilevs, Y.: Isogeometric analysis: CAD, finite elements, NURBS, exact geometry and mesh refinement. *Comput. Methods Appl. Mech. Eng.*, 194(39-41), 4135-4195 (2005)
- [18] Johnson, C., & Pitkäranta, J.: An analysis of the discontinuous Galerkin method for a scalar hyperbolic equation. *Math. Comp.*, 46(173), 1-26 (1986)
- [19] Kawecki, E. L.: Finite element theory on curved domains with applications to discontinuous Galerkin finite element methods. *Numer. Methods Partial Differential Equations*, 36(6), 1492-1536 (2020)
- [20] Lathrop, K. D.: Use of discrete-ordinates methods for solution of photon transport problems. *Nucl. Sci. Eng.*, 24(4), 381-388 (1966)
- [21] Lebaud, M. P.: Error estimate in an isoparametric finite element eigenvalue problem. *Math. Comp.*, 63(207), 19-40 (1994)
- [22] Lehtikangas, O., Tarvainen, T., Kim, A. D., & Arridge, S. R.: Finite element approximation of the radiative transport equation in a medium with piece-wise constant refractive index. *J. Comput. Phys.*, 282, 345-359 (2015)
- [23] Lenoir, M.: Optimal isoparametric finite elements and error estimates for domains involving curved boundaries. *SIAM J. Numer. Anal.*, 23(3), 562-580 (1986)
- [24] Lesaint, P., & Raviart, P. A.: On a finite element method for solving the neutron transport equation. *Publ. Semin. Math. Inform. Rennes*, (S4), 1-40 (1974)
- [25] Li, B., Xia, Y., & Yang, Z.: Optimal convergence of arbitrary Lagrangian-Eulerian isoparametric finite element methods for parabolic equations in an evolving domain. *IMA J. Numer. Anal.*, 43(1), 501-534 (2023)
- [26] Li, L., Su, H., Zhang, H., & Zheng, W.: A divergence-free parametric finite element method for 3D Stokes equations on curved domains. *arXiv preprint arXiv:2512.16216* (2025)

- [27] Modest, M. F., & Mazumder, S.: Radiative heat transfer. Academic Press (2021)
- [28] Nedoma, J.: The finite element solution of elliptic and parabolic equations using simplicial isoparametric elements. *RAIRO Anal. Numer.*, 13(3), 257-289 (1979)
- [29] Pazner, W., & Haut, T.: A short note on the accuracy of the discontinuous Galerkin method with reentrant faces. *J. Comput. Phys.*, 443, 110448 (2021)
- [30] Peterson, T. E.: A note on the convergence of the discontinuous Galerkin method for a scalar hyperbolic equation. *SIAM J. Numer. Anal.*, 28(1), 133-140 (1991)
- [31] Richter, G. R.: An optimal-order error estimate for the discontinuous Galerkin method. *Math. Comp.*, 50(181), 75-88 (1988)
- [32] Riviere, B.: Discontinuous Galerkin methods for solving elliptic and parabolic equations: theory and implementation. Society for Industrial and Applied Mathematics (2008)
- [33] Rybicki, G. B., & Lightman, A. P.: Radiative processes in astrophysics. John Wiley & Sons (2024)
- [34] Sevilla, R., Fernandez-Mendez, S., & Huerta, A.: NURBS-enhanced finite element method (NEFEM). *Int. J. Numer. Methods Eng.*, 76(1), 56-83 (2008)
- [35] Thomas, G. E., & Stamnes, K.: Radiative transfer in the atmosphere and ocean. Cambridge University Press (2002)
- [36] Zhang, L. B. A parallel algorithm for adaptive local refinement of tetrahedral meshes using bisection. *Numer. Math. Theory Methods Appl.*, 2(1), 65-89 (2009)